

# ‘Stückelberg interferometry’ with ultracold molecules

M. Mark,<sup>1</sup> T. Kraemer,<sup>1</sup> P. Waldburger,<sup>1</sup> J. Herbig,<sup>1</sup> C. Chin,<sup>1,3</sup> H.-C. Nägerl,<sup>1</sup> R. Grimm<sup>1,2</sup>

<sup>1</sup>*Institut für Experimentalphysik und Forschungszentrum für Quantenphysik, Universität Innsbruck, 6020 Innsbruck, Austria*

<sup>2</sup>*Institut für Quantenoptik und Quanteninformation,*

*Österreichische Akademie der Wissenschaften, 6020 Innsbruck, Austria*

<sup>3</sup>*Physics Department and James Franck Institute, University of Chicago, Chicago, IL 60637, USA*

(Dated: August 18, 2021)

We report on the realization of a time-domain ‘Stückelberg interferometer’, which is based on the internal state structure of ultracold Feshbach molecules. Two subsequent passages through a weak avoided crossing between two different orbital angular momentum states in combination with a variable hold time lead to high-contrast population oscillations. This allows for a precise determination of the energy difference between the two molecular states. We demonstrate a high degree of control over the interferometer dynamics. The interferometric scheme provides new possibilities for precision measurements with ultracold molecules.

PACS numbers: 34.50.-s, 05.30.Jp, 32.80.Pj, 67.40.Hf

The creation of molecules on Feshbach resonances in atomic quantum gases has opened up a new chapter in the field of ultracold matter [1]. Molecular quantum gases are now readily available in the lab for various applications. Prominent examples are given by the creation of strongly interacting many-body systems based on molecular Bose-Einstein condensates [2], experiments on few-body collision physics [3], the realization of molecular matter-wave optics [4], and by the demonstration of exotic pairs in optical lattices [5]. Recent experimental progress has shown that full control over all degrees of freedom can be expected for such molecules [6, 7, 8]. Ultracold molecular samples with very low thermal spread and long interaction times could greatly increase the sensitivity in measurements of fundamental physical properties such as the existence of an electron dipole moment [9] and a possible time-variation of the fine-structure constant [10, 11].

Most of today’s most accurate and precise measurements rely on interferometric techniques applied to ultracold atomic systems. For example, long coherence times in atomic fountains or in optical lattices allow ultraprecise frequency metrology [12, 13]. Molecules, given their rich internal structure, greatly extend the scope of possible precision measurements. Molecular clocks, for example, may provide novel access to fundamental constants and interaction effects, different from atomic clocks. The fast progress in preparing cold molecular samples thus opens up fascinating perspectives for precision interferometry. Recently, the technique of Stark deceleration has allowed a demonstration of Ramsey interferometry with a cold and slowed molecular beam [10]. Ultracold trapped molecular ensembles are expected to further enhance the range of possible measurements.

In this Letter, we report on the realization of an internal-state interferometer with ultracold Cs<sub>2</sub> molecules. A weak avoided crossing is used as a ‘beam splitter’ for molecular states as a result of partial Landau-Zener tun-

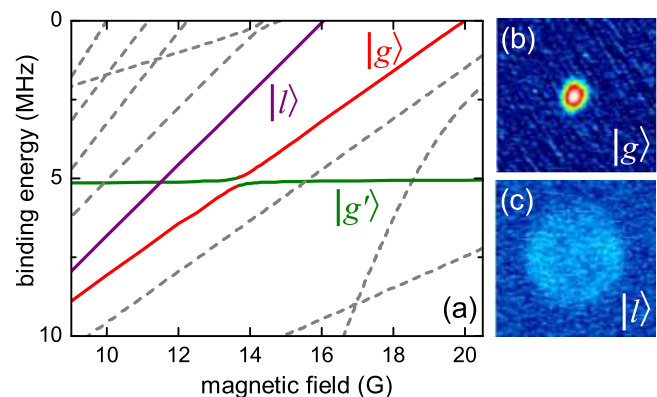


FIG. 1: (color online). (a) Molecular energy structure below the dissociation threshold showing all molecular states up  $\ell = 8$ . The relevant states for the present experiment (solid lines) are labeled  $|g\rangle$ ,  $|g'\rangle$ , and  $|l\rangle$ . Molecules in state  $|g\rangle$  or  $|l\rangle$  are detected upon dissociation as shown in (b) and (c). The crossing used for the interferometer is the one between  $|g'\rangle$  and  $|l\rangle$  near 11.4 G. Initially, ultracold molecules are generated in state  $|g\rangle$  on the Feshbach resonance at 19.8 G.

neling when it is traversed by means of an appropriately chosen magnetic field ramp. Using the avoided crossing twice, first for splitting, and then for recombination of molecular states, leads to the well-known ‘Stückelberg oscillations’ [14]. We thus call our scheme a ‘Stückelberg interferometer’. Our realization of this interferometer allows full control over the interferometer dynamics. In particular, the hold time between splitting and recombination can be freely chosen. In analogy to the well-known Ramsey interferometer [15] the acquired interferometer phase is mapped onto the relative populations of the two output states that can be well discriminated upon molecular dissociation. To demonstrate the performance of the Stückelberg interferometer we use it for precision molecular spectroscopy to determine the position and coupling strength of the avoided crossing.

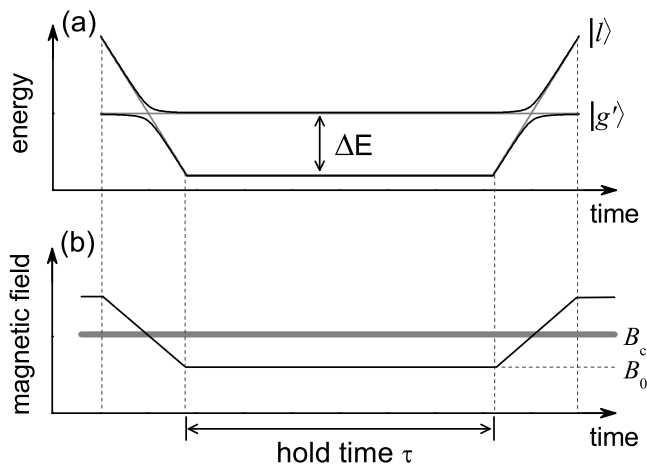


FIG. 2: (a) Scheme of the ‘Stückelberg interferometer’. By ramping the magnetic field over the avoided crossing at  $B_c$  at a rate near the critical ramp rate  $R_c$  the population in the initial molecular state is coherently split.  $\Delta E$  is the binding energy difference at the given hold field  $B_0$ . After the hold time  $\tau$  a reverse ramp coherently recombines the two populations. The populations in the two ‘output ports’ are then determined as a function of acquired phase difference  $\phi \propto \Delta E \times \tau$ . (b) Corresponding magnetic field ramp.

The energy structure of weakly bound  $\text{Cs}_2$  dimers in the relevant range of low magnetic field strength is shown in Fig. 1 [16]. Zero binding energy corresponds to the threshold of dissociation into two free Cs atoms in the lowest hyperfine sublevel  $|F=3, m_F=3\rangle$  and thus to the zero-energy collision limit of two atoms. The states relevant for this work are labelled by  $|g\rangle$ ,  $|g'\rangle$ , and  $|l\rangle$  [17]. While  $|g\rangle$  and  $|g'\rangle$  are  $g$ -wave states with orbital angular momentum  $\ell=4$ , the state  $|l\rangle$  is an  $l$ -wave state with a high orbital angular momentum of  $\ell=8$  [18]. Coupling with  $\Delta\ell=4$  between  $s$ -wave atoms and  $g$ -wave molecules and between  $g$ - and  $l$ -wave states is a result of the strong indirect spin-spin interaction between two Cs atoms [16].

The starting point for our experiments is a Bose-Einstein condensate (BEC) with  $\sim 2 \times 10^5$  Cs atoms in the  $|F=3, m_F=3\rangle$  ground state confined in a crossed-beam dipole trap generated by a broad-band fiber laser with a wavelength near 1064 nm [19, 20]. The BEC allows us to efficiently produce molecules on a narrow Feshbach resonance at 19.84 G [21] in an optimized scheme as described in Ref. [22]. With an efficiency of typically 25% we produce a pure molecular ensemble with up to  $2.5 \times 10^4$  ultracold molecules all in state  $|g\rangle$ , initially close to quantum degeneracy [21]. The following experiments are performed on the molecular ensemble in free fall. During the initial expansion to a  $1/e$ -diameter of about  $28 \mu\text{m}$  along the radial and about  $46 \mu\text{m}$  along the axial direction the peak density is reduced to  $1 \times 10^{11} \text{cm}^{-3}$  so that molecule-molecule interactions [3] can be neglected on the timescale of the experiment.

The molecules can now be transferred to any one of the molecular states shown in Fig. 1 with near 100% efficiency by controlled ‘jumping’ or adiabatic following at the various crossings [23]. When the magnetic field strength is decreased, the molecules first encounter the crossing at 13.6 G. At all ramp rates used in our present experiments the passage through this crossing takes place in a fully adiabatic way. The molecules are thus transferred from  $|g\rangle$  to  $|g'\rangle$  along the upper branch of the crossing. They then encounter the next crossing at a magnetic field of  $B_c \approx 11.4$  G. We accidentally found this weak crossing in our previous magnetic moment measurements [3, 23]. This allowed the identification of the  $l$ -wave state  $|l\rangle$  [18].

This crossing between  $|g'\rangle$  and  $|l\rangle$  plays a central role in the present experiment. It can be used as a tunable ‘beam splitter’, which allows adiabatic transfer, coherent splitting, as will be shown below, or diabatic transfer for the molecular states involved, depending on the chosen magnetic ramp rate near the crossing. We find that a critical ramp rate of  $R_c \approx 14 \text{ G/ms}$  leads to a 50/50-splitting into  $|g'\rangle$  and  $|l\rangle$  [23]. Using the well-known Landau-Zener formula and an estimate for the difference in magnetic moment for states  $|g'\rangle$  and  $|l\rangle$  [18] we determine the coupling strength  $V$  between  $|g'\rangle$  and  $|l\rangle$  to  $\sim h \times 15 \text{ kHz}$ .

We state-selectively detect the molecules by ramping up the magnetic field to bring the molecules above the threshold for dissociation. There the quasi-bound molecules decay into the atomic scattering continuum. For state  $|g\rangle$  dissociation is observed for magnetic fields above the 19.84 G position of the corresponding Feshbach resonance. Fig. 1 (b) shows a typical absorption image of the resulting atom cloud [21]. For state  $|l\rangle$  dissociation is observed above 16.5 G. The molecular states can thus be easily discriminated by the different magnetic field values needed for dissociation. Moreover, the expansion pattern is qualitatively different from the one connected to state  $|g\rangle$ . The absorption image in Fig. 1 (c) shows an expanding ‘bubble’ of atoms with a relatively large kinetic energy of about  $k_B \times 20 \mu\text{K}$  per atom. Here,  $k_B$  is Boltzmann’s constant. We find that significant dissociation occurs only when the state  $|l\rangle$  couples to a quasi-bound  $g$ -wave state about  $h \times 0.7 \text{ MHz}$  above threshold [24]. The resulting bubble is not fully spherically symmetric, which indicates higher partial-wave contributions [25]. The different absorption patterns allow us to clearly distinguish between the two different dissociation channels in a single absorption picture when the magnetic field is ramped up to  $\sim 22$  G. These dissociation channels serve as the interferometer ‘output ports’.

The interferometer is based on two subsequent passages through the crossing following the scheme illustrated in Fig. 2. For an initial magnetic field above the crossing a downward magnetic-field ramp brings the initial molecular state into a coherent superposition of  $|g'\rangle$  and  $|l\rangle$ . After the ramp the field is kept constant at a

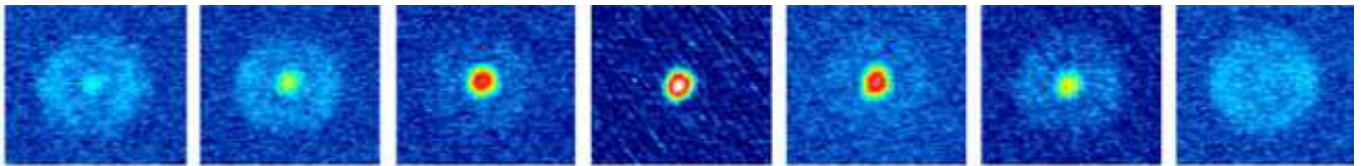


FIG. 3: (color online). Series of dissociation patterns showing about one oscillation period with  $\Delta E/h = 155$  kHz at a hold field of 11.19 G. From one picture to the next the hold time  $\tau$  is increased by  $1 \mu\text{s}$ . The first and the last of the absorption images mainly show dissociation of  $l$ -wave molecules, whereas the central image shows predominant dissociation of  $g$ -wave molecules.

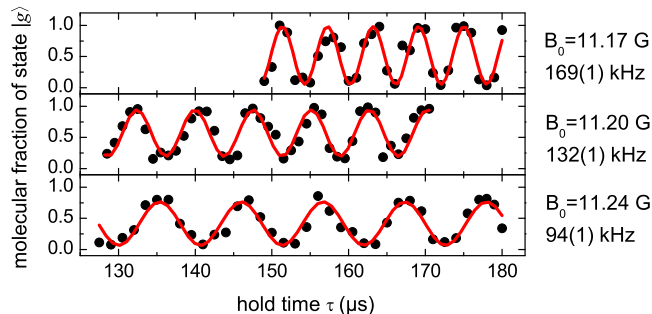


FIG. 4: Interferometer fringes for magnetic hold fields  $B_0$  below the crossing of  $|g'\rangle$  and  $|l\rangle$ . The  $g$ -wave molecular fraction is plotted as a function of the hold time  $\tau$ . Sinusoidal fits give the oscillation frequency as indicated.

hold field  $B_0$  below the crossing for a variable hold time  $\tau$ . A differential phase  $\phi$  is then accumulated between the two components, which linearly increases with the product of the binding energy difference  $\Delta E$  and the hold time  $\tau$ . The magnetic field is then ramped back up, and the second passage creates a new superposition state depending on  $\phi$ . For a 50/50-splitting ratio, this can lead to complete destructive or constructive interference in the two output ports and thus to high-contrast fringes as a function of  $\tau$  or  $\Delta E$ . These fringes, resulting from two passages through the same crossing, are analogous to the well-known Stückelberg oscillations in collision physics [14, 26] or in the physics with Rydberg atoms [27, 28]. Note that our realization of a ‘Stückelberg interferometer’ gives full control over the interferometer dynamics by appropriate choice of ramp rates and magnetic offset fields.

A typical ramp sequence, as shown in Fig. 2 (b), starts with a sample of  $|g'\rangle$  molecules at a magnetic field of 11.6 G about 250 mG above the crossing. At the critical ramp rate  $R_c$  we ramp the magnetic field within about  $50 \mu\text{s}$  to a hold field  $B_0$  below the crossing. After the variable hold time  $\tau$  we reverse the ramp and transverse the crossing a second time at the critical ramp rate. The output of the interferometer is detected by rapidly ramping the magnetic field up to 22 G and by imaging the pattern of dissociating  $|l\rangle$  and  $|g\rangle$  molecules.

For one period of oscillation the dependence of the dissociation pattern on the hold time  $\tau$  is demonstrated by

the series of absorption images shown in Fig. 3. The hold time is increased in steps of  $1 \mu\text{s}$  while the entire preparation, ramping, and detection procedure is repeated for each experimental cycle, lasting about 20 s. The molecular population oscillates from being predominantly  $l$ -wave to predominantly  $g$ -wave and back. For a quantitative analysis of the molecular population in each output port we fit the images with a simple model function [29] and extract the fraction of molecules in each of the two output ports. Fig. 4 shows the  $g$ -wave molecular population as a function of hold time  $\tau$  for various hold fields  $B_0$  corresponding to different  $\Delta E$ . The existence of these Stückelberg oscillations confirms that coherence is preserved by the molecular beam splitter. Their high contrast ratio shows that near 50/50-splitting is achieved. Sinusoidal fits to the data allow for an accurate determination of the oscillation frequency and hence of  $\Delta E$ .

Fig. 5 shows  $\Delta E$  as a function of magnetic field strength near the avoided crossing. For magnetic fields below the crossing we obtain  $\Delta E$  as described before. For magnetic fields above the crossing, we invert the interferometric scheme. Molecules are first transferred from  $|g'\rangle$  into  $|l\rangle$  using a slow adiabatic ramp. The field is then ramped up above the crossing with a rate near  $R_c$ , kept constant for the variable time  $\tau$  at the hold field  $B_0$  and then ramped down to close the interferometer. An adiabatic ramp through the crossing maps population in  $|g'\rangle$  onto  $|l\rangle$  and vice versa. Detection then proceeds as before.

For both realizations of the interferometer we obtain high-contrast fringes even when it is not operated in the Landau-Zener regime and the fast ramps are stopped right at the crossing (see inset to Fig. 5). This allows us to measure  $\Delta E$  in the crossing region. A fit to the data with a hyperbolic fit function according to the standard Landau-Zener model yields  $B_c = 11.339(1)$  G for the position of the crossing,  $\Delta\mu = 0.730(6) \mu_B$  for the difference in magnetic moment of the two states involved ( $\mu_B$  is Bohr’s magneton), and  $V = h \times 14(1)$  kHz for the coupling strength. While the measured  $\Delta\mu$  agrees reasonably well with the result from an advanced theoretical model of the  $\text{Cs}_2$  dimer [18],  $B_c$  and  $V$  cannot be obtained from these calculations with sufficient accuracy.

The present interferometer allows us to observe up to 100 oscillations at 200 kHz. Shot-to-shot fluctuations in-

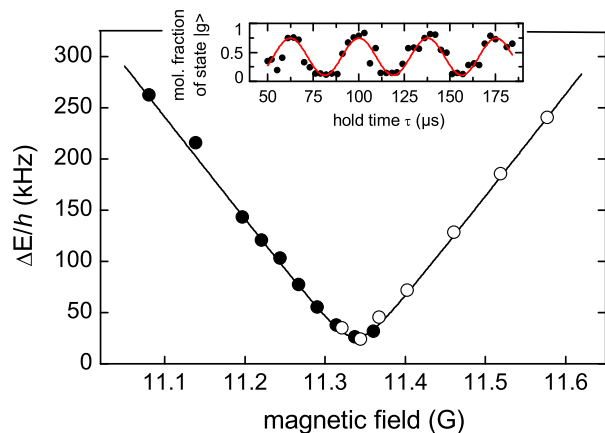


FIG. 5: Interferometrically measured binding energy difference  $\Delta E$  in the region of the crossing between states  $|g'\rangle$  and  $|l\rangle$  as a function of magnetic field. Solid circles: Standard ramp sequence of the interferometer. Open circles: Inverted scheme for field values above the crossing. The one-sigma statistical error from the sinusoidal fit is less than the size of the symbols. The solid curve is a hyperbolic fit to the experimental data. Inset: Oscillation at 26.6(3) kHz for a hold field  $B_0 = 11.34$  G right on the crossing.

creasingly scramble the phase of the oscillations for longer hold times until the phase appears to be fully randomized while large amplitude variations for the molecular populations persist. The peak-to-peak amplitude of these fluctuations decays slowly and is still 50% of the initial contrast after 1 ms. We attribute this phase scrambling to magnetic field noise that causes shot-to-shot variations of  $\Delta E$ , the same, however, for each molecule. The large amplitude of these fluctuations indicates that phase coherence is preserved within the molecular sample. We attribute the gradual loss of peak-to-peak amplitude to spatial magnetic field inhomogeneities. We expect that straightforward technical improvements regarding the magnetic field stability and homogeneity and applying the interferometer to trapped molecular samples will allow us extend the hold times far into the millisecond range. It will then be possible to measure ultraweak crossings with coupling strengths well below  $h \times 1$  kHz.

We have demonstrated a molecular Stückelberg interferometer with full control over the interferometer dynamics. The interferometer can be used as a spectroscopic tool as it allows precise measurements of binding energy differences of molecular states. In particular, the technique can be employed to measure feeble interactions between molecular states, such as parity non-conserving interactions [30]. The sensitivity to detect ultraweak level crossings, combined with long storage times in optical molecule traps [3] or lattices [5, 6, 7], may allow to detect interaction phenomena on the  $h \times 1$  Hz scale. In view of the rapid progress in various preparation methods for cold molecular samples, new tools for precision mea-

surements on molecular samples, such as our Stückelberg interferometer, will open up exciting avenues for future research.

We thank E. Tiesinga for discussions and for theoretical support. We acknowledge financial support by the Austrian Science Fund (FWF) within SFB 15 (project part 16) and by the EU within the Cold Molecules TMR Network under contract No. HPRN-CT-2002-00290. M.M. and C.C. acknowledge support by DOC [PhD-Program of the Austrian Academy of Science] and the FWF Lise-Meitner program, respectively.

- 
- [1] For a review, see T. Köhler, K. Góral, and P.S. Julienne, *Rev. Mod. Phys.* **78**, 1311 (2006).
  - [2] See e.g. *Ultracold Fermi Gases*, Proceedings of the International School of Physics “Enrico Fermi”, Course CLXIV, Varenna, 20 - 30 June 2006, edited by M. Inguscio, W. Ketterle, and C. Salomon, in press.
  - [3] C. Chin *et al.*, *Phys. Rev. Lett.* **94**, 123201 (2005).
  - [4] J.R. Abo-Shaeer *et al.* *Phys. Rev. Lett.* **94**, 040405 (2005).
  - [5] K. Winkler *et al.*, *Nature* **441**, 853 (2006).
  - [6] G. Thalhammer *et al.*, *Phys. Rev. Lett.* **96**, 050402 (2006).
  - [7] T. Volz *et al.*, *Nature Physics* **2**, 692 (2006).
  - [8] K. Winkler *et al.*, *Phys. Rev. Lett.* **98**, 043201 (2007).
  - [9] J. J. Hudson, B. E. Sauer, M. R. Tarbutt, and E. A. Hinds, *Phys. Rev. Lett.* **89**, 023003 (2002).
  - [10] E. R. Hudson, H. J. Lewandowski, B. C. Sawyer, and J. Ye, *Phys. Rev. Lett.* **96**, 143004 (2006).
  - [11] C. Chin and V. V. Flambaum, *Phys. Rev. Lett.* **96**, 230801 (2006).
  - [12] S. Bize *et al.*, *J. Phys. B* **38**, S449 (2005).
  - [13] M. M Boyd *et al.*, *Phys. Rev. Lett.* **98**, 083002 (2007).
  - [14] E.C.G. Stückelberg, *Helv. Phys. Acta* **5**, 369 (1932).
  - [15] N.F. Ramsey, *Molecular Beams* (Oxford University Press, London, 1956).
  - [16] C. Chin *et al.*, *Phys. Rev. A* **70**, 032701 (2004).
  - [17] Using the notation  $|f, m_f; l, m_l\rangle$  of Ref. [16], the three states  $|g\rangle$ ,  $|g'\rangle$ , and  $|l\rangle$  correspond to  $|4, 4; 4, 2\rangle$ ,  $|6, 6; 4, 0\rangle$ , and  $|6, 3; 8, 3\rangle$ , respectively.
  - [18] E. Tiesinga (private communication).
  - [19] T. Kraemer *et al.*, *Appl. Phys. B* **79**, 1013 (2004).
  - [20] T. Weber *et al.*, *Science* **299**, 232 (2003).
  - [21] J. Herbig *et al.*, *Science* **301**, 1510 (2003).
  - [22] M. Mark *et al.*, *Europhys. Lett.* **69**, 706 (2005).
  - [23] M. Mark *et al.*, manuscript in preparation.
  - [24] S. Knoop *et al.*, manuscript in preparation.
  - [25] S. Dürr, T. Volz, and G. Rempe, *Phys. Rev. A* **70**, 031601(R) (2004).
  - [26] E. E. Nikitin and S. Ya. Umanskii, *Theory of Slow Atomic Collisions* (Springer, Berlin, 1984).
  - [27] M. C. Baruch and T. F. Gallagher, *Phys. Rev. Lett.* **68**, 3515 (1992).
  - [28] S. Yoakum, L. Sirko, and P. M. Koch, *Phys. Rev. Lett.* **68**, 1919 (1992).
  - [29] We model the dissociation pattern with appropriately chosen spherical harmonic functions to account for the angular distribution [25].

[30] E. D. Commins, *Adv. At. Mol. Opt. Phys.* **40**, 1 (1999).